



Effect of combined multi-cell columns and exterior stiffeners on energy absorption parameters of thin-walled tubes under axial load

Ali Akhavan Attar¹ · S. A. Rasouli² · S. Chahardoli¹

Received: 31 January 2020 / Accepted: 27 July 2020 / Published online: 11 August 2020
© The Brazilian Society of Mechanical Sciences and Engineering 2020

Abstract

In this paper, the energy absorption parameters are investigated for new forms of thin-walled energy absorbers. The effect of adding stiffeners to the outer tube wall, as well as the multi-cell effect of the structure, was investigated both in a separate and simultaneous manner in a tube with the square section. This design has not been investigated in previous studies, and it stimulates innovation in its own right. Such designs can significantly increase the energy absorption of the structure with the least change in the initial geometry and the lowest costs. The nonlinear explicit finite element method was used to simulate the crushing process in the tubes. The numerical simulation results were validated with the results of experimental tests, and a good agreement was observed. Finally, the parameters such as specific energy absorption, crush force efficiency, initial peak force, and mean crush force were calculated and analyzed. The results showed that the proper combination of stiffeners in the middle sides of the tube wall and the creation of a multi-cell column made it possible to improve the specific energy absorption up to 89% and crush force efficiency up to 52% compared with the reference tube, which is a significant improvement. Also, while comparing some of the results, it was analyzed why sometimes inserting stiffeners on the outer wall of tubes is better than the multi-cell method to increase the SEA of structure.

Keywords Thin-walled tube · SEA · LS DYNA · Stiffeners · Multi-cell columns

1 Introduction

Today, the use of thin-walled structures that dissipate energy through plastic deformation is expanding. These absorbers are employed to protect structures and reduce damages and failures caused by collision [1–4]. They have different types that absorb energy in various ways. Among them, the more suitable absorbers are the tube structures which are progressively crushed. This is due to the high energy absorption efficiency, low weight, and low cost of these structures. The aluminum alloys are used as energy absorbers in various forms, the most important reason for the high aluminum

strength-to-weight ratio. The higher the absorber deformation, the higher the energy absorption level. However, the amount of energy absorbed by each structure should be compared and evaluated proportional to its mass [5–8]. Three important and effective parameters can be considered in the investigation of energy absorbers, including amount of absorbed energy per unit mass that is called specific energy absorption (SEA), the peak crushing force that is usually occurred at the beginning of the crushing process, and the crush force efficiency (CFE) that can be considered as a measure of the force stability in the impact process. The research background about the thin-walled energy absorbers is very extensive, and some of the activities related to the topic are as follows.

For the first time, Alexander examined the axial loading of thin-walled circular tubes [9]. Since then, the folding of thin-walled tubes was introduced as a mechanism for energy absorption. The first experimental tests and theoretical investigations for examining the tubes with the circle and square sections were carried out in the quasi-static and dynamic

Technical editor: João Marciano Laredo dos Reis.

✉ S. A. Rasouli
s.a.rasouli@malayeru.ac.ir; seyedalirezarasouli@gmail.com

¹ Department of Mechanical Engineering, Bu-Ali Sina University, Hamedan, Iran

² Department of Mechanical Engineering, Faculty of Engineering, Malayer University, Malayer, Iran

modes by Abramowicz and Wierzbicki [10, 11], Abramowicz and Jones [12, 13], and Andrew et al. [14].

Recently, the useful and improving effects of multi-cell sections on the specific energy absorption (SEA) of structures led to the diverse and attractive research on multi-cell sections comparing the single-cell ones. This research was carried out on the structures with different geometric sections such as circle, square, and rectangle, where the effect of various factors such as filling the structure with foam was investigated. This research also investigated the effect of various loading types such as axial, lateral, and oblique loadings on the energy absorption of these structures [15–25]. The experimental and numerical studies confirmed that the multi-cell sections have a higher energy absorption efficiency than single-cell sections [26–29]. In a comparative study, Xiong Zhang and Hui Zhang [17, 18, 20] applied the quasi-static axial loads to multi-cell tubes. The results of the experiment were compared with numerical simulation, and it was found that the specific energy absorption in the multi-cell columns was significantly higher than single-cell tubes. Birch and Jones [30] conducted experimental tests to investigate the effect of length, location, and number of stiffeners (external and internal) on the energy absorption of thin-walled cylinders. This research did not have an analytical and numerical study. Zhang and Suzuki [31] investigated the effect of external stiffeners on the mean crush force (mean load) in the thin-walled square sections under quasi-static loading. Finally, by performing multiple numerical simulations and experiments, a relation was presented to calculate the mean crush force.

In this paper, the effect of multi-cell columns combined with external stiffeners on the energy absorption of a thin-walled structure with square section is investigated. Although in the previous studies, the energy absorbers with square sections were studied in different ways, the idea behind combining the multi-cell and a number of stiffeners to the outer walls of these structures for enhancing the energy absorption parameters can be innovative. This design has not been investigated in previous studies, and it stimulates innovation in its own right. In addition, such designs can significantly increase the energy absorption of the structure with the least change in the initial geometry and the lowest costs.

2 Experimental study

2.1 Specimen specifications

The experimental tests were conducted to validate the results of numerical simulations and also to determine the material properties required for the accurate numerical simulations.

To compare the energy absorption rates of different samples, an energy absorber with a simple square section and without multi-cell columns and external stiffeners was selected as the reference tube, as shown in Fig. 1, which is designated as “RT”.

Figure 2 shows the geometric sections considered for different samples. The rectangular stiffeners have a width of 20 mm and a thickness of 1.5 mm added to each sample. The number after “C” shows the number of stiffeners in the corner, and the number after “M” is the number of stiffeners in the middle sides. Three types of multi-cell columns are considered for the structure that is seen as a cross, plus, and square from the top view, and are designated as “-C”, “-P” and “-S” to distinguish the sample notations. For example, the sample code C4M8-P means that there are four stiffeners in the corners and eight stiffeners in the middle sides, and the multi-cell column inside is seen as a plus sign (+) from the top view.

Four models of the samples presented in Fig. 2 were selected for setting up and performing the experimental tests: RT, C4M4, C4M8, and C8M4. The samples were constructed through sheeting, bending, and finally welding. The cutting and bending pattern of the sheets was done in such a way that it would be less to the welding lines to produce the final sample.

According to the ASTM E826, quantometric test was performed on primary material according to standard (Table 1). The structural material of the tubes is AA1200. Obtaining better results as well as avoiding the rupture of parts during the experiments, necessitate the annealing of the primary aluminum through heat treatment. In Fig. 3, two tested

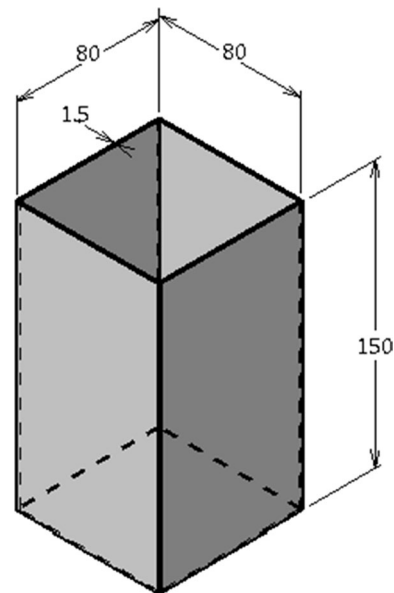
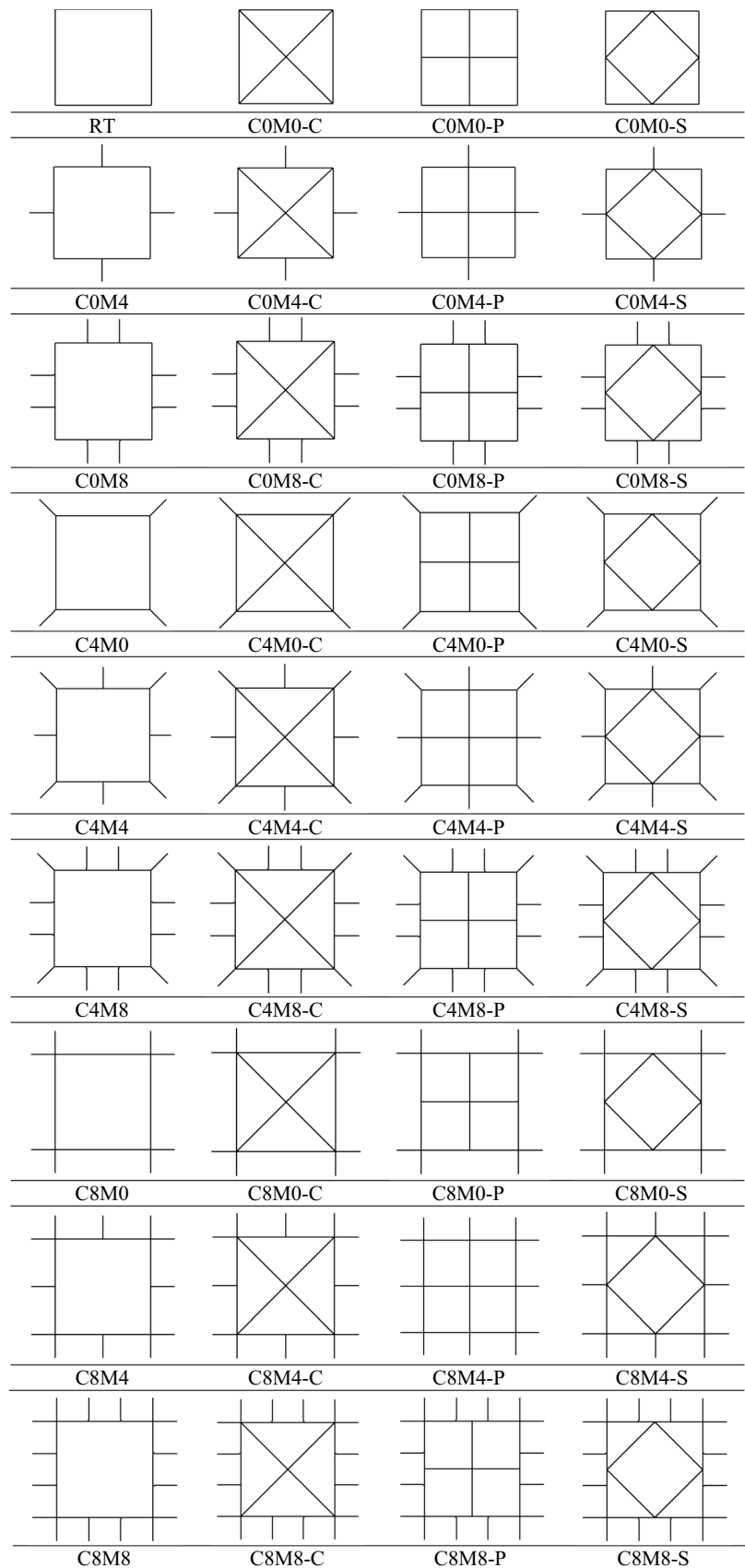


Fig. 1 RT sample dimensions (mm)

Fig. 2 Geometric section of samples from the top view



specimens: annealed specimen and specimen without heat treatment, are depicted. As can be seen, the rupture has occurred in the second specimen.

For obtaining the data concerning the material hardening for the tubes, it was intended to conduct tensile tests according to ASTM E8M standard. Prepared specimens for the tensile test, the specimen during the test, and the

specimen after the test are presented in Fig. 4. The tensile tests were conducted at a speed of 2 mm/min. Moreover, an extensometer was used for calculating the precise values of elastic modulus.

The representative engineering stress–strain curves for AA1200 tubes are plotted in Fig. 5 in the two states before and after annealing. The mechanical properties of

Table 1 Comparison of quantometric test results with ASTM standard

Element	Si+Fe	Cu	Mn	Zn	Others (each)	Others (total)	Al
Standard percent for AA1200	1.0 Max	0.05–0.2	0.05 Max	0.1 Max	0.05 Max	0.15 Max	Rem
Tested Plate	0.05 0.15	0.01	0.01	0.1	Ok	Ok	Ok

Fig. 3 **a** Annealed specimen, and **b** without heat treatment

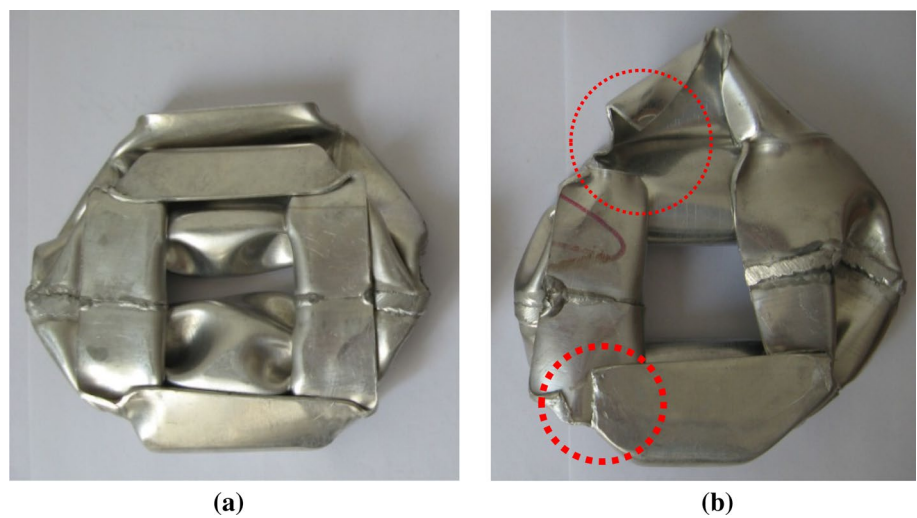
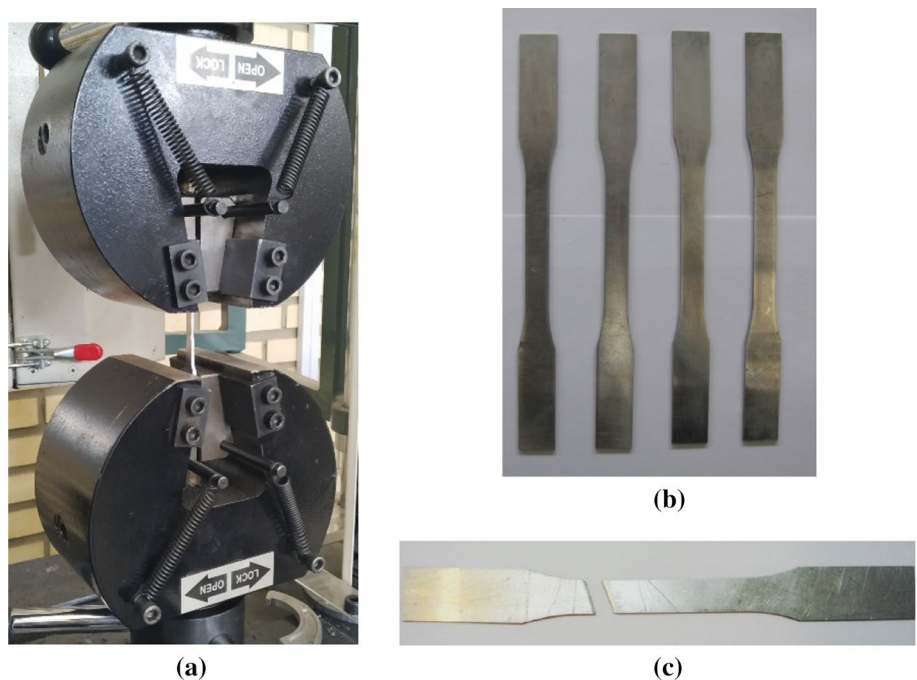


Fig. 4 **a** tensile test sample during loading, **b** tensile test specimens, **c** after tensile test



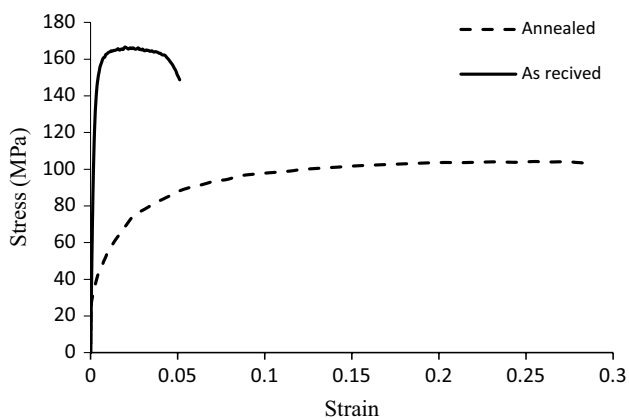


Fig. 5 Stress–strain curve for AA1200 before and after annealing

the material AA1200-annealed are also presented here: initial yield stress $\sigma_y = 39$ MPa, ultimate stress $\sigma_u = 103$ MPa, Young’s modulus $E = 69$ GPa, and Poisson’s ratio $\nu = 0.3$.

2.2 Quasi-static tests

The specimens were prepared by bending and Argon arc welding of 1.5 mm thick aluminum sheets. In Fig. 6, the preparation of the specimens for the tests is shown. For obtaining the clamped condition, the bottom of each column was welded to a thick aluminum plate.

The energy absorption parameters were obtained through the loading tests of the specimens by the STM 150KN test device. The device was equipped with computer control and data acquisition systems. The compression jaws were

installed, and the specimen was fixed on the device. The compression test was conducted by the downward motion of the upper jaw toward the fixed lower jaw with a speed of 20 mm/min. Each test was repeated twice, and the mean value was reported. The force–displacement diagram was obtained from the performed tests, from which, the SEA can be determined.

Crushing steps of the RT sample are indicated in Fig. 7 to the final level of 120 mm. The mass of specimens prior to the tests, as well as the corresponding specific energy absorption, are listed in Table 2.

3 Numerical investigation

For the numerical study of the energy absorption parameters, LS-DYNA finite element software was utilized. The quasi-static loading was modeled through the explicit analysis; quasi-static loading condition was finished at the desired time by the use of time step analysis. Moreover, the loading speed was selected to be to 1 m/s regarding the study of Santosa et al. [32].

The material behavior of the tube was defined by MAT-PIECWIES-LINEAR-PLASTICITY-TITLE in order to define a stress–strain curve consisting of up to eight linear segments, while MAT-RIGID-TITLE was used for the determination of the plate material behavior. Therefore, the rigid material model with a density of 7800 kg/m³, Young’s modulus of 210 GPa, and Poisson’s ratio of 0.3 was attributed to these parts. The material behavior was specified through the true stress–true strain diagram, which was obtained from

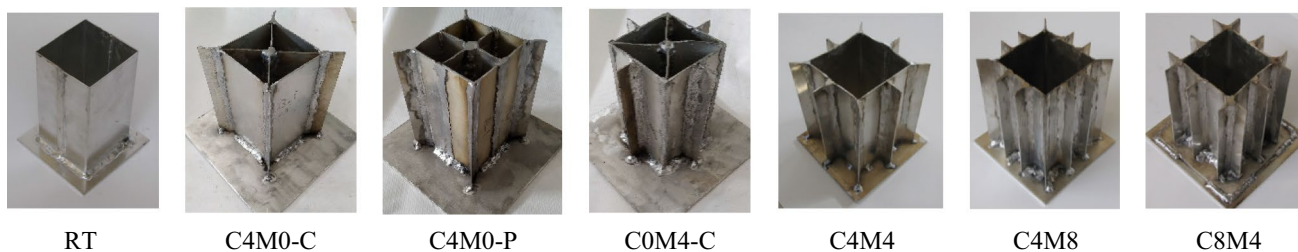


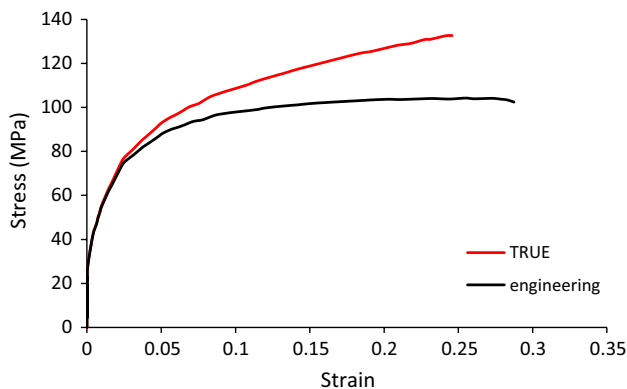
Fig. 6 Fabricated specimens



Fig. 7 Consecutive steps of sample deformation

Table 2 Experimental data from tests

Specimen code	Peak load (N)	Mean Load (N)	SEA (J/g)	Mass (g)	Energy (J)
RT	23,255	10,052	6.20	197	1222
C4M0-C	48,399	26,057	7.86	380	2986
C4M0-P	45,322	28,157	9.53	339	3230
C8M4	51,226	26,537	8.77	361	3167
C4M4	39,454	23,732	9.16	315	2888
C4M8	53,988	31,812	10.68	368	3931

**Fig. 8** True stress–strain curve for numerical simulation

the tensile testing (Fig. 5). The following equations were used to obtain the true strain–stress data for use in numerical simulation:

$$\sigma_{\text{True}} = \sigma_{\text{Eng}}(1 + \epsilon_{\text{Eng}}) \quad (1)$$

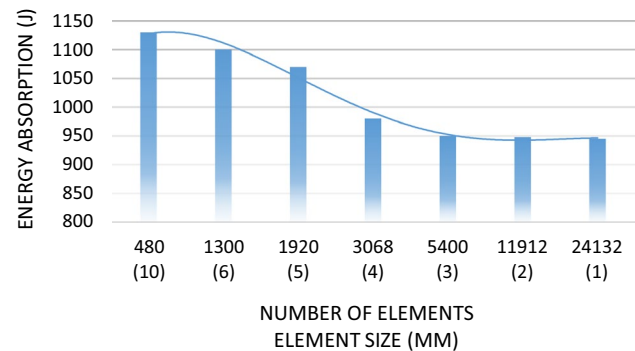
$$\epsilon_{\text{True}} = \ln(1 + \epsilon_{\text{Eng}}) \quad (2)$$

In Fig. 8, the true and engineering stress–strain curves are plotted and compared.

The tube was simulated by the shell elements through the Belytschko-Tsay formulation due to its satisfactory results in quasi-static simulation. Different numbers of tube elements were examined to evaluate the sensitivity of the absorbed energy. As can be seen in Fig. 9, the four-node square elements with the dimensions of 2 mm represent the best results.

The Automatic_Surface_to_Surface was selected for simulating the contact between the jaws and the structure. Additionally, to prevent the slippage of the rigid wall and tube, the coefficient of friction was chosen to be 0.3. Moreover, to prevent element–element penetration, Automatic_Single_Surface was selected for the contact between tube elements. The designed finite element model for the absorber is depicted in Fig. 10.

The downward movement of the upper jaw in a quasi-static manner towards the fixed lower jaw is shown in Fig. 7.

**Fig. 9** Mesh convergence for RT energy absorption

The boundary conditions should also be revised in accordance with the restraining of the bottom of the tube, which was fulfilled by restraining the corresponding nodes in the simulation. The presented specimens in Fig. 2 were simulated by this procedure.

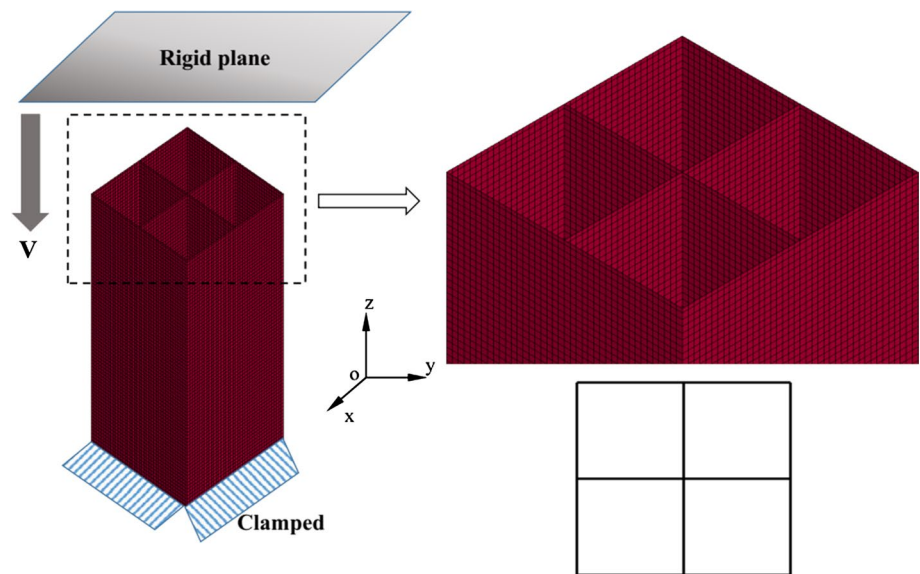
4 Results and discussion

4.1 Validation of numerical simulation results

One of the important issues for ensuring the accuracy of numerical simulation results is to compare the results obtained from the load–displacement diagrams. Figure 11 shows comparison of the diagrams obtained from the experimental test on four samples with the numerical simulation results by the help of the obtained diagrams, the demanded parameters, including specific energy absorption (SEA), peak crush load, mean crush load, and crush force efficiency (CFE) can be calculated. The CFE can be determined by dividing the mean load to the peak load. This parameter is always in the range of zero and one. For the values close to one, a more uniform crush load would be obtained during the compression of the structure, which is desired.

As can be seen in the diagrams, there is a good agreement between the experimental mode and the numerical simulations. A comparison of the summary of results for Fig. 11 is given in Table 3. The calculation of the difference in this table is based on the experimental test results.

Fig. 10 Representative finite element model for tubes



The lowest error for the calculation of SEA is about 1.4% related to the C4M0-C. The highest error is 8%, which is related to C8M4. The main causes of errors can be due to the welding done on the sample, material behavior not being ideal in the experimental mode, low distortion in the structure stiffeners due to the thermal stress entered during the sample preparation, or the deviation in the geometric symmetry and displacement of plastic hinges in the experimental mode.

As shown in Table 3, the SEA value in simulation is always higher than the experimental test. The reason for this phenomenon can be the ideal material and the geometric details of structure in the simulation, which plays an effective role in the regular crush of the structure and maximizes the specific energy absorption. On the other hand, the non-perfect material and geometric models of the tested specimens helped to exacerbate this phenomenon.

It is also evident that the initial force is lower about 6–10% in the experimental mode compared with the numerical simulation. This trend has been repeated in all diagrams and there is no exception, and therefore, a rational reason should be found for this case. It seems that the material assumed by the software as aluminum in the numerical simulation is ideal, and there exists no pore. Therefore, it would be logical during the crush that the initial peak force for starting the folding in the simulation mode to be higher than that in the experimental mode. Generally, the reduction in the initial peak force is caused by the triggers above the structures. However, for the welded specimens, this process will reduce the initial force, and there is no need to create a trigger.

The number of peaks in the simulation and experimental modes is almost the same for all of the load–displacement diagrams. Each peak in the load–displacement diagram

represents the formation of a plastic hinge during the structure crush, which will cause the folding of a specimen.

To perform a better comparison of the behavior of each structure after the loading, some images were taken from the crushed samples, and then, they were placed alongside the images obtained from the LS-Dyna. Figure 12 shows this comparison. The crush pattern and the geometric behavior between the experimental test and numerical simulation are very similar to each other, which is another proof of the accuracy of numerical simulation results.

4.2 Comparison of energy absorption parameters

A numerical simulation was performed for all structures of Fig. 2, the results of which are presented in Fig. 13 and Table 4. The important parameters of energy absorption were accurately calculated. Figure 14 shows the specific energy absorption (SEA) values for different samples, and Fig. 15 displays the changes in the crush force efficiency.

In order to investigate the effect of stiffeners on the energy absorption of structures, the non-multi-cell samples should be compared in terms of SEA and CFE parameters. The results show that samples C0M8, C4M8, and C8M8 have 77, 76, and 77% higher specific energy absorption than RT, respectively, which have the highest SEA among the non-multi-cell samples. This increase is due to an increase in the mean load. In fact, the mean load has increased greatly, while the mass of the structure has not increased as much. Also, the values of the CFE parameter in the three samples were increased 41, 39, and 44% relative to the RT, respectively, which were the highest values among the non-multi-cell samples. The feature in common with the three samples is the placement of eight stiffeners in the middle sides of the square section. Therefore, increasing the number of

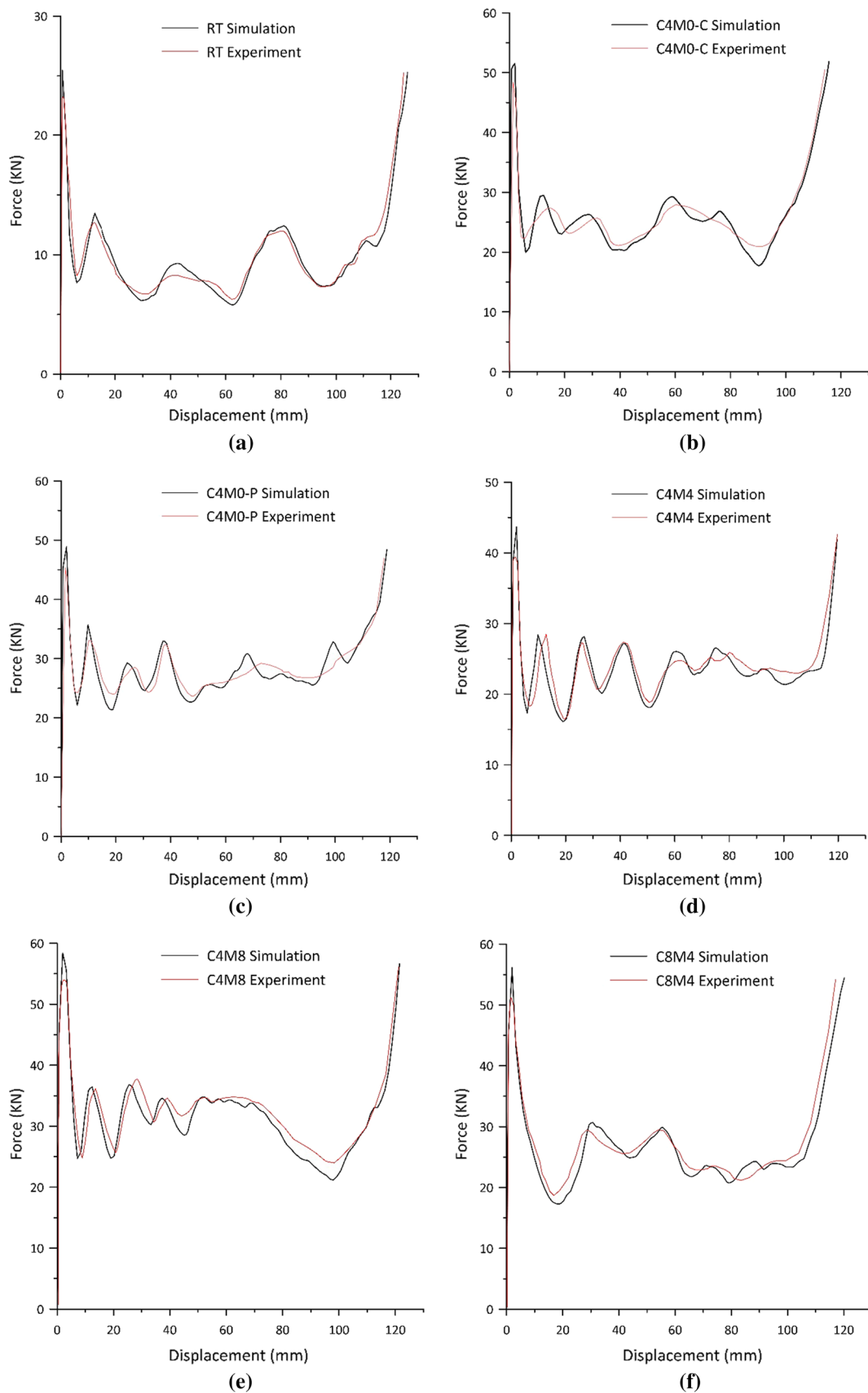


Fig. 11 Comparison of load–displacement diagram in numerical simulation with experimental mode: **a** RT, **b** C4M0-C, **c** C4M0-P, **d** C4M4, **e** C4M8, **f** C8M4

Table 3 Comparison between experimental data and simulation results

	Specimen code	SEA (J/g)	Difference (%)	Initial Peak Load (N)	Difference (%)
RT	FE	6.39	3.0	25,487	9.5
	Experiment	6.20		23,255	
C4M0-C	FE	7.97	1.4	51,534	6.0
	Experiment	7.86		48,399	
C4M0-P	FE	9.98	4.5	48,899	7.8
	Experiment	9.53		45,322	
C4M4	FE	9.66	5.4	43,661	10.6
	Experiment	9.16		39,454	
C4M8	FE	11.26	5.4	58,427	8.2
	Experiment	10.68		53,988	
C8M4	FE	9.48	8.0	56,181	9.6
	Experiment	8.77		51,226	

stiffeners in the middle sides led to the improved performance of energy absorber, while increasing the number of stiffeners in the corners did not have a significant effect on the increase in the SEA. This is because the stiffeners in the middle of the sides of the structure, in addition to absorbing energy when they are crushed, also partially prevent the side surfaces of the structure from buckling.

It should be noted that although the total energy absorption in the C8M8 is significantly higher than the C0M8, the greater mass of the C8M8, as compared with C0M8, caused that their specific energy absorption to be almost identical.

The multi-cell method is not always the best way to increase the SEA of structure. Sometimes, creating stiffeners in the outer wall of samples is a better way to increase the SEA of structure. For example, the SEA in C0M8 is larger than that in all C0M4-C, C0M4-P and C0M4-S samples, and even more than some of the corresponding multi-cell samples, namely C0M8-C and C0M8-S. Another useful comparison is the multi-cell sample C0M0-P, which is identical to the C0M8 in terms of weight, but C0M8 has 23% more SEA and also 10% higher CFE. Therefore, in some designs for the thin-walled structures, instead of multi-cell structures, it is possible to increase the specific energy absorption and the crush force efficiency by finding the best location for the stiffeners in the outer wall of the structure. This is possible without increasing the mass of the structure and even with its reduction, which is desirable in the design of thin-walled structures.

One important point in examining the results is that for the samples that were identical in terms of the arrangement of stiffeners but different in terms of multi-cell column type, it can be argued firmly and without exception that the samples with the multi-cell column of type “P” always have the highest specific energy absorption and highest crush force

efficiency. In addition, a multi-cell column of type “P” always imposes less mass on the structure compared with the types “C” and “S”, and therefore, it is also better in terms of design and production cost.

According to Table 4, the C0M8-P had the highest SEA and highest CFE values of 12.10 and 0.59, respectively. Therefore, this sample can be considered the best structure among the studied structures in terms of energy absorption, which increased the SEA value by 89% compared with the simple sample with a square section (RT). Regarding the energy absorption of thin-walled structures, the 89% increase in SEA is considered to be significant. Also, the CFE value in the C0M8-P was 52% higher than the RT, which is a significant value, and the C0M8-P in this case also outperforms the rest of the samples.

Figure 16 compares the load–displacement diagram of RT and C0M8-P. Given the fact that the area below the load–displacement diagram shows the total energy absorption of the structure, the colored area between the two diagrams represents the difference in the total energy absorption of the two samples. As shown in Fig. 16, the C0M8-P absorbed 3468 joules of energy more than the RT, which represents a 279% increase. Figure 17 shows the C0M8-P before and after the crush, and also reveals the folding pattern and overlapping in a cut section of the structure.

For the samples without the stiffener (C0M0-C, S, P), the multi-cell method has a direct relationship with the increase in the crush force efficiency, and in these samples, the multi-cell column of type “S” is better than “P” and the type “P” is better than “C” ($S > P > C$). However, in the presence of stiffeners, CFE of mesh type “P” is often better than or almost equal to the type “S”. Generally, it can be stated that the samples with type “C” multi-cell column do not have a desirable CFE, because type “C” meshes have a higher

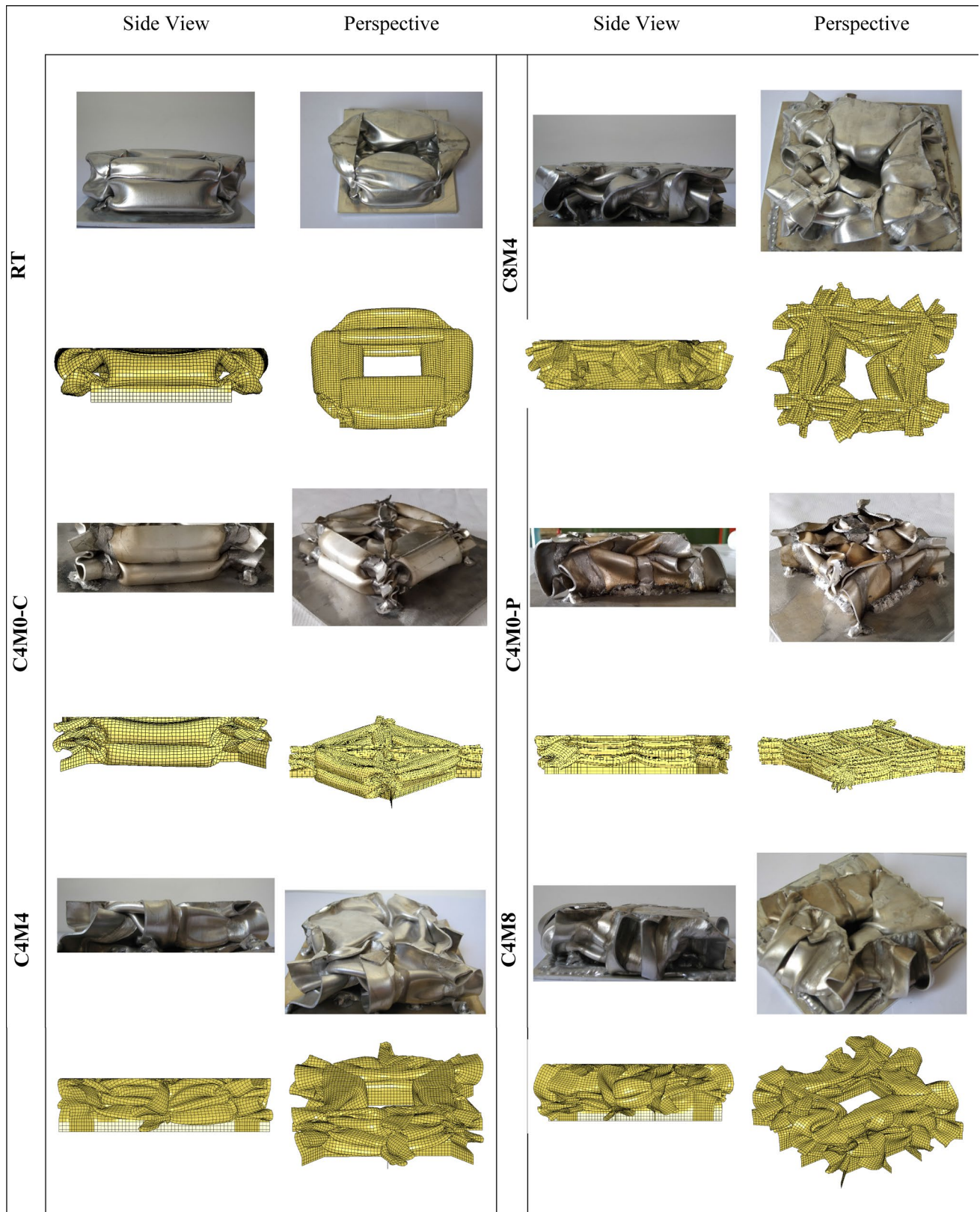


Fig. 12 Comparison of structural deformation (experimental test and simulation)

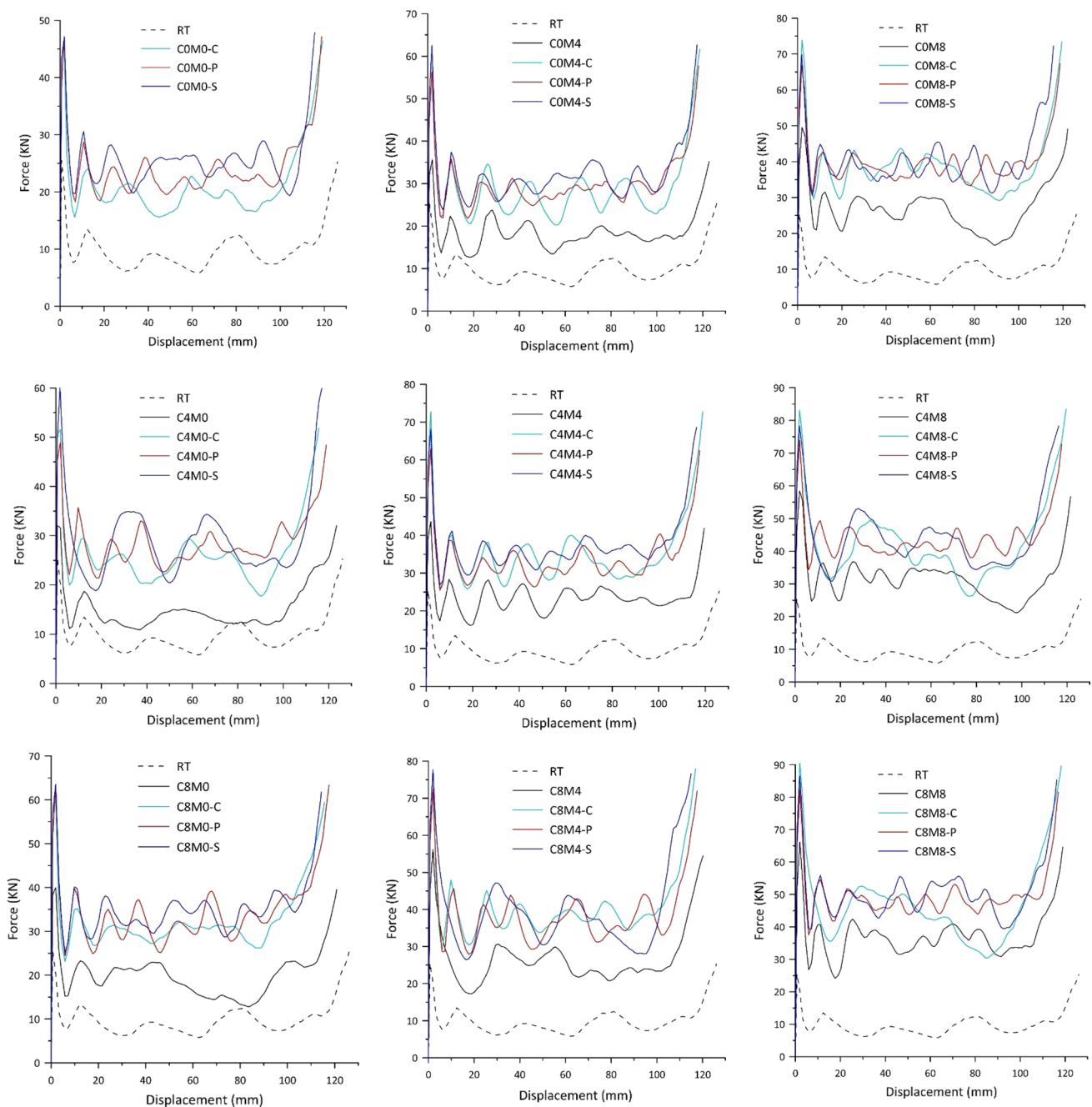


Fig. 13 Load–displacement curves of the samples compared with RT(numerical simulation)

initial peak load compared with the type “P” mesh, while creating a little mean load during the structure crush process. Altogether, simultaneously taking the values of SEA and CFE into account, it is clear that choosing the proper arrangement of stiffeners along with the multi-cell column of type “P” produces the best performance, which is better than other geometric patterns of Fig. 2 to be used as an energy absorber.

It should be noted that the higher SEA and CFE values in a structure than those in the other structure necessarily do not mean having higher values of peak load and mean load. This is because the weight factor is involved in calculating the SEA, and in the calculation of CFE, the effect of peak load to mean load ratio would be involved. Therefore, a structure with a good energy absorption is one that has a

Table 4 Results from numerical simulation of samples

Specimen	Mass (g)	Energy (J)	SEA (J/g)	Mean Load (N)	Peak Load (KN)	CFE
RT	194	1239	6.39	9864	25,487	0.39
C0M0-C	332	2550	7.68	21,374	46,751	0.46
C0M0-P	291	2855	9.81	24,008	47,194	0.51
C0M0-S	332	2950	8.89	25,484	46,991	0.54
C0M4	243	2272	9.35	18,492	35,593	0.52
C0M4-C	380	3407	8.97	28,876	61,866	0.47
C0M4-P	340	3527	10.37	29,808	56,322	0.53
C0M4-S	380	3769	9.92	32,019	62,506	0.51
C0M8	292	3297	11.29	26,943	49,536	0.54
C0M8-C	429	4646	10.83	38,795	73,894	0.53
C0M8-P	389	4707	12.10	39,392	66,774	0.59
C0M8-S	429	4694	10.94	40,473	69,800	0.58
C4M0	243	1879	7.73	15,234	32,017	0.48
C4M0-C	380	3028	7.97	26,184	51,534	0.51
C4M0-P	340	3394	9.98	28,487	48,899	0.58
C4M0-S	380	3413	8.98	29,165	60,051	0.49
C4M4	292	2821	9.66	23,559	43,661	0.54
C4M4-C	429	4183	9.75	35,147	72,739	0.48
C4M4-P	389	3964	10.19	33,657	63,121	0.53
C4M4-S	429	4324	10.08	37,120	68,184	0.54
C4M8	340	3829	11.26	31,457	58,427	0.54
C4M8-C	478	5080	10.63	42,433	83,114	0.51
C4M8-P	438	5160	11.78	43,751	73,940	0.59
C4M8-S	478	5182	10.84	44,463	78,272	0.57
C8M0	292	2426	8.31	20,074	39,950	0.50
C8M0-C	429	3761	8.77	32,486	59,912	0.54
C8M0-P	389	4011	10.31	34,052	62,850	0.54
C8M0-S	429	4028	9.39	35,177	63,561	0.55
C8M4	340	3223	9.48	26,793	56,181	0.48
C8M4-C	478	4739	9.91	40,462	77,808	0.52
C8M4-P	438	4523	10.33	38,395	72,478	0.53
C8M4-S	478	4594	9.61	39,900	77,582	0.51
C8M8	389	4407	11.33	36,975	66,162	0.56
C8M8-C	527	5577	10.58	47,079	90,491	0.52
C8M8-P	486	5753	11.84	49,052	82,294	0.59
C8M8-S	527	5887	11.17	50,488	86,577	0.58

lower weight and better energy absorption parameters, while having a simple and cost-effective design.

5 Conclusions

The purpose of this study was to investigate the energy absorption of thin-walled aluminum square structures, and the new designs were suggested for the section geometry. These structures were subjected to axial loading after installing the stiffeners in the outer wall of the structure by creating

various multi-cell columns at the inner surface. The effect of the number and arrangement of stiffeners in the structure wall, type of multi-cell columns, and the stiffeners combined with multi-cell column were investigated in this study. A total of 36 different modes were examined and numerically simulated. The simulations were performed with the LS-DYNA finite element software, and for the validation of simulation results, it was necessary to compare the absorbed energy values and the load–displacement diagrams with the corresponding values in several laboratory samples. To perform the verification, the laboratory samples made of

Fig. 14 Specific energy absorption (SEA) values of different samples in numerical simulation

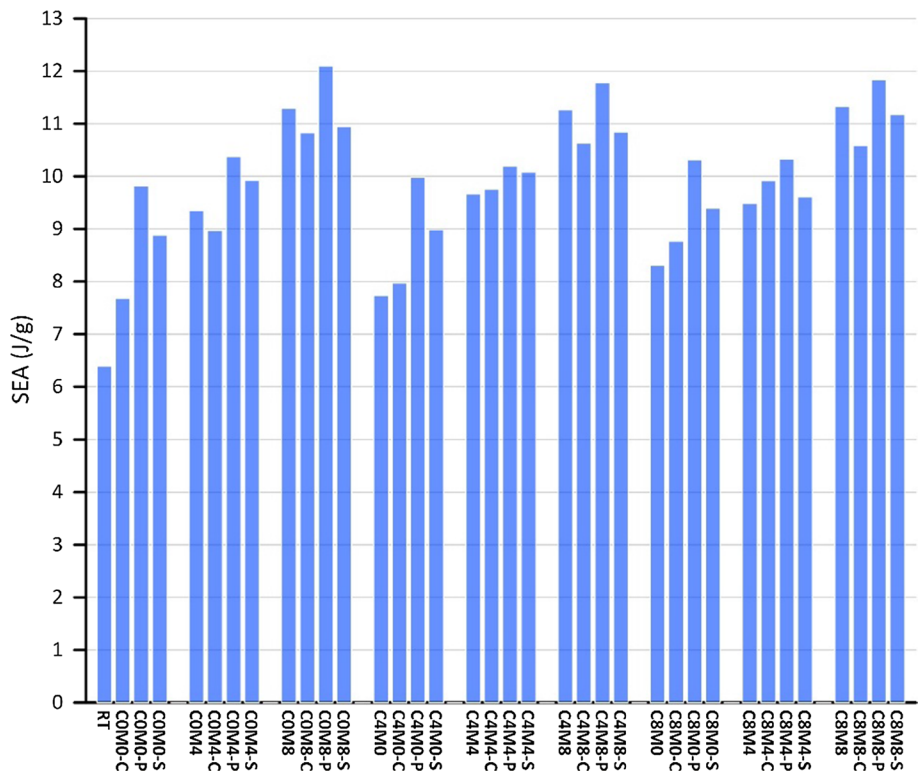
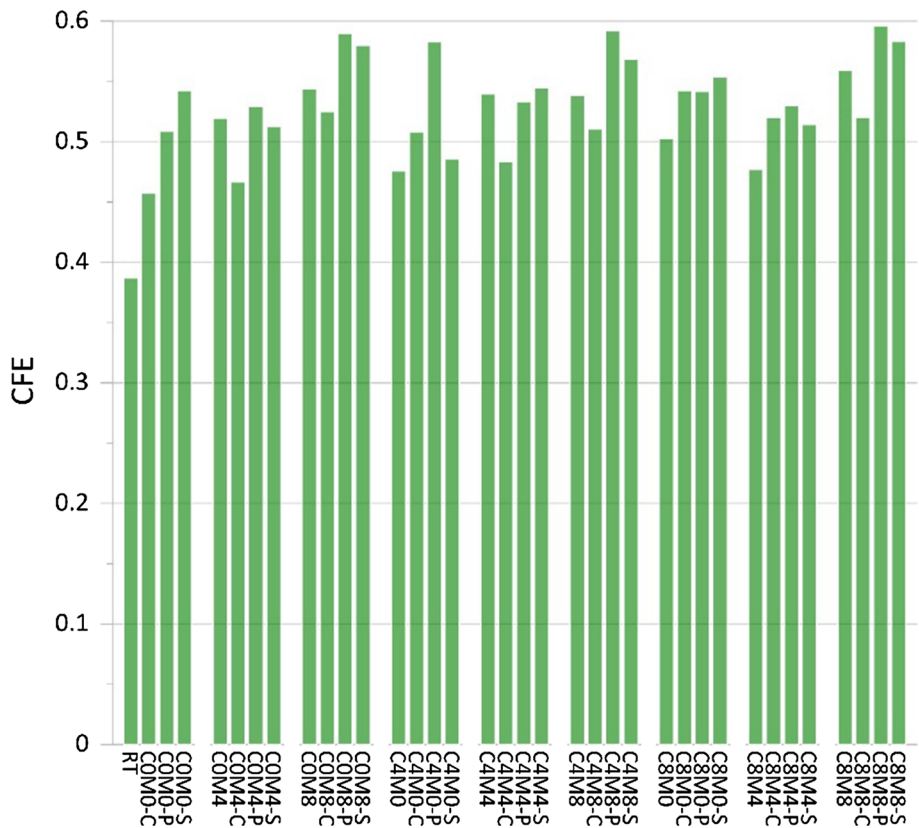


Fig. 15 Crush force efficiency (CFE) values for different samples in numerical simulation



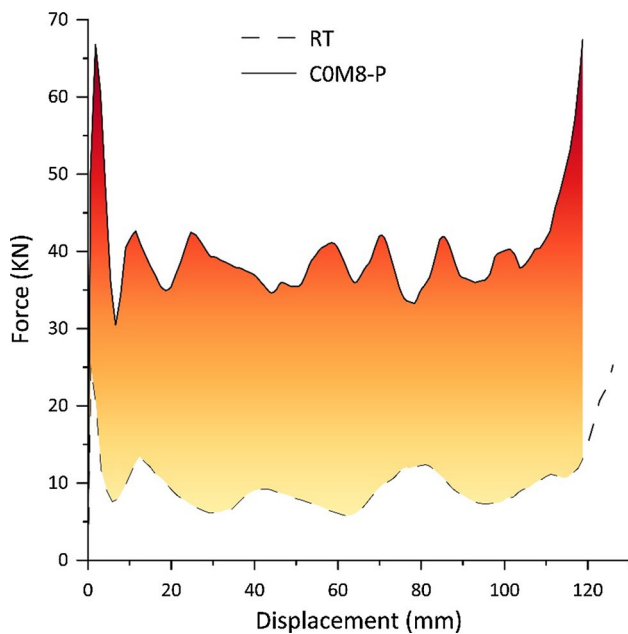


Fig. 16 Load–displacement diagram of samples RT and COM8-P and difference in absorbed energy

aluminum were subjected to quasi-static axial loading, and there was a good agreement between the results. In addition to simple installation and replacement, the energy absorbers should be affordable with lower weight, if possible. Some of the designs presented in this study by creating multi-cell columns in the structure and adding the proper arrangement of stiffeners simply improved the energy absorption of the structure to a satisfactory level with the least weight gain. The summary of the most important results of this research is as follows:

- The best structure among the studied ones was COM8-P, which had the highest amount of SEA and CFE equal to 12.10 and 0.59, respectively. In this sample, the amount of SEA was increased by 89% compared with the RT.
- The COM8-P absorbed 3468 joules of energy more than the RT, which represents a 279% increase.
- Creating a multi-cell column is not necessarily the best way to increase the SEA of structure. Sometimes, the installation of stiffeners in the outer wall of the structure is a better way to increase the SEA of structure. The samples COM4, COM8 and C8M8 were in this category.
- For the samples without the stiffener (COM0-C, S, P), the multi-cell method has a direct relationship with the increase in the crush force efficiency, and in these samples, the multi-cell column of type “S” is better than “P” and the type “P” is better than “C” ($S > P > C$).
- Among the samples without a multi-cell column, the samples COM8, C4M8 and C8M8 had 77, 76 and 77% specific energy absorption higher than the RT, respectively. The CFE of the three samples was increased 41, 39 and 44%, which is the highest CFE value among the samples without the multi-cell column.
- In the samples that were identical in terms of the arrangement of the stiffeners, but differ in terms of the type of multi-cell column, the samples with the type “P” multi-cell column always had the highest SEA and the highest CFE.
- In general, the samples with the type “C” multi-cell column do not have a desirable crush force efficiency, because the CFE values have always been less than the values related to “P” and “S” types.

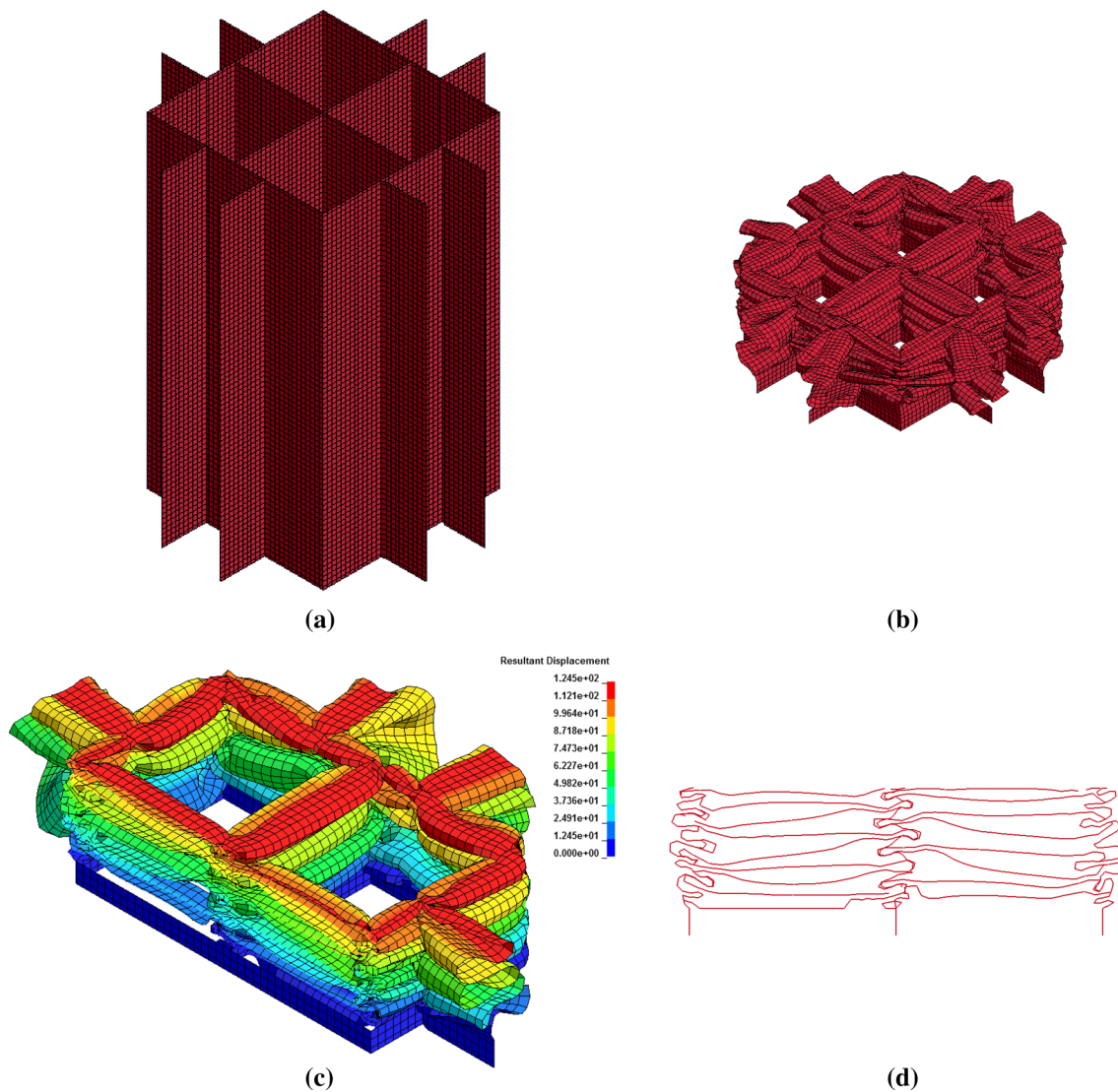


Fig. 17 **a** Isometric view of C0M8-P before crushing, **b** isometric view of C0M8-P after crushing, **c** profile of displacement contour in C0M8-P, **d** folding pattern and overlapping from the front view of a cut section in the image **c**

References

- Gan N, Yao S, Dong H et al (2018) Energy absorption characteristics of multi-frusta configurations under axial impact loading. *Thin-Walled Structures* 122:147–157
- Sun G, Pang T, Xu C et al (2017) Energy absorption mechanics for variable thickness thin-walled structures. *Thin-Walled Struct* 118:214–228
- Jafarian N, Rezvani MJ (2019) Crushing behavior of multi-component conical tubes as energy absorber: a comparative analysis between end-capped and non-capped conical tubes. *Eng Struct* 178:128–135
- Fu J, Liu Q, Liufu K et al (2019) Design of bionic-bamboo thin-walled structures for energy absorption. *Thin-Walled Struct* 135:400–413
- Florence A, Gefken P, Kirkpatrick S (1991) Dynamic plastic buckling of copper cylindrical shells. *Int J Solids Struct* 27(1):89–103
- Wierzbicki T, Bhat SU, Abramowicz W et al (1992) Alexander revisited—a two folding elements model of progressive crushing of tubes. *Int J Solids Struct* 29(24):3269–3288
- Gupta N, Velmurugan R (1995) An analysis of axi-symmetric axial collapse of round tubes. *Thin-Walled Struct* 22(4):261–274
- Seifi R, Chahardoli S, Akhavan Attar A (2017) Axial buckling of perforated plates reinforced with strips and middle tubes. *Mech Res Commun* 85:21–32
- Alexander J (1960) An approximate analysis of the collapse of thin cylindrical shells under axial loading. *Q J Mech Appl Math* 13(1):10–15
- Abramowicz W, Wierzbicki T (1989) Axial crushing of multi-corner sheet metal columns. *J Appl Mech* 56(1):113–120
- Wierzbicki T, Abramowicz W (1983) On the crushing mechanics of thin-walled structures. *J Appl Mech* 50(4a):727–734
- Abramowicz W, Jones N (1984) Dynamic axial crushing of square tubes. *Int J Impact Eng* 2(2):179–208

13. Abramowicz W, Jones N (1986) Dynamic progressive buckling of circular and square tubes. *Int J Impact Eng* 4(4):243–270
14. Andrews K, England G, Ghani E (1983) Classification of the axial collapse of cylindrical tubes under quasi-static loading. *Int J Mech Sci* 25(9):687–696
15. Chen W, Wierzbicki T (2001) Relative merits of single-cell, multi-cell and foam-filled thin-walled structures in energy absorption. *Thin-Walled Struct* 39(4):287–306
16. Najafi A, Rais-Rohani M (2011) Mechanics of axial plastic collapse in multi-cell, multi-corner crush tubes. *Thin-Walled Struct* 49(1):1–12
17. Zhang X, Zhang H (2013) Energy absorption of multi-cell stub columns under axial compression. *Thin-Walled Struct* 68:156–163
18. Zhang X, Zhang H (2013) Energy absorption limit of plates in thin-walled structures under compression. *Int J Impact Eng* 57:81–98
19. Tang Z, Liu S, Zhang Z (2013) Analysis of energy absorption characteristics of cylindrical multi-cell columns. *Thin-Walled Struct* 62:75–84
20. Zhang X, Zhang H (2014) Axial crushing of circular multi-cell columns. *Int J Impact Eng* 65:110–125
21. Tran T, Hou S, Han X et al (2014) Theoretical prediction and crashworthiness optimization of multi-cell square tubes under oblique impact loading. *Int J Mech Sci* 89:177–193
22. Jusuf A, Dirgantara T, Gunawan L et al (2015) Crashworthiness analysis of multi-cell prismatic structures. *Int J Impact Eng* 78:34–50
23. Tabacu S (2015) Axial crushing of circular structures with rectangular multi-cell insert. *Thin-Walled Struct* 95:297–309
24. Yin H, Xiao Y, Wen G et al (2015) Multiobjective optimization for foam-filled multi-cell thin-walled structures under lateral impact. *Thin-Walled Struct* 94:1–12
25. Wang Z, Li Z, Zhang X (2016) Bending resistance of thin-walled multi-cell square tubes. *Thin-Walled Struct* 107:287–299
26. Yu H, Shi H, Chen S (2019) A novel multi-cell CFRP/AA6061 hybrid tube and its structural multiobjective optimization. *Composite Structures* 209:579–589
27. Chen J, Fang H, Liu W et al (2018) Energy absorption of foam-filled multi-cell composite panels under quasi-static compression. *Compos Part B: Eng* 153:295–305
28. Yang K, Xu S, Zhou S et al (2018) Multi-objective optimization of multi-cell tubes with origami patterns for energy absorption. *Thin-Walled Struct* 123:100–113
29. Sun G, Liu T, Huang X et al (2018) Topological configuration analysis and design for foam filled multi-cell tubes. *Eng Struct* 155:235–250
30. Birch R, Jones N (1990) Dynamic and static axial crushing of axially stiffened cylindrical shells. *Thin-Walled Struct* 9(1):29–60
31. Zhang A, Suzuki K (2007) A study on the effect of stiffeners on quasi-static crushing of stiffened square tube with non-linear finite element method. *Int J Impact Eng* 34(3):544–555
32. Santosa SP, Wierzbicki T, Hanssen AG et al (2000) Experimental and numerical studies of foam-filled sections. *Int J Impact Eng* 24(5):509–534

Publisher's Note Springer Nature remains neutral with regard to jurisdictional claims in published maps and institutional affiliations.